JOURNAL OF SCIENCE AND TECHNOLOGY
ISSN: 2229-8460 e-ISSN: 2600-7924

JST

Vol. 16 No. 2 (2024) 71-84
https://publisher.uthm.edu.my/ojs/index.php/jst

Evaluation of a Mechanistic Model and Finite Element Analysis for Geosynthetic-Reinforced Sub-grade Material Performance under Cyclic Loading

Ali RamazanBorujerdi[1]*

[1] *Department of Civil Engineering,*
Qom University of Technology, Tehran, 1651958171, IRAN

*Corresponding Author: aliborujerdi1371@gmail.com
DOI: https://doi.org/10.30880/jst.2024.16.02.009

Article Info

Received: 29 August 2024
Accepted: 3 November 2024
Available online: 21 November 2024

Keywords

Sub-grade soil, triaxial tests, CBR, geosynthetic reinforced, cyclic loading, finite element method (FEM), pavement, AASHTO

Abstract

This study investigates the outcomes of triaxial repeated loading tests on geosynthetic reinforced base course materials intended for road construction. Triaxial testing was utilized to simulate the impact of traffic loads. Two types of samples were examined: one set without reinforcement and another with reinforcement. The research included a thorough series of tests that varied parameters such as density, moisture content, initial effective stress, and cyclic loading conditions. The findings can be illustrated through deformation and failure envelopes applicable to various cycle counts. Factors such as the material's compaction level, moisture content, and saturation degree significantly affect its deformability. An elastic-plastic analysis utilizing the finite element method (FEM) was conducted to validate the experimental results and to establish the parameters necessary for the FEM analysis of the pavement. Utilizing the principles outlined in the AASHTO pavement design methodology, the necessary combined load-bearing capacity of the pavement layers situated above the sub-grade was determined. Additionally, the AASHTO geosynthetic reinforced roadway design approach was established. The mechanical properties, specifically strength and stiffness of reinforced with geosynthetics at various elevations were assessed through both static and cyclic triaxial testing methods. It was noted that the positive impacts of reinforcement were closely linked to the amount of reinforcement used, with the advantages of geosynthetic reinforcement becoming particularly apparent at higher strain levels.

1. Introduction

Soil improvement could be an important solution for foundations on problematic soils. Austin [1] provides five main soil conditioning functions applied to foundations: Increasing load-bearing capacity, controlling deformation and accelerating consolidation, providing lateral stability to slopes and excavations, shutting off leachate and other types of environmental control, and increasing resistance to liquefaction of loose and saturated granular deposits. Geosynthetics, as an emerging technology, has been widely utilized to reduce reflective cracking in paved roadways. Recent studies have assessed the role of Geosynthetics as reinforcement components in asphalt overlays, with the objective of improving the mechanical characteristics of both newly constructed and rehabilitated pavements increase [2]. Over the last three decades, the utilization of geosynthetics to enhance flexible pavement systems has seen a notable increase [2]. Generally, geosynthetic

reinforcement is installed at the junctions between the aggregate base course and the sub-grade; however, it may also be applied at the interfaces of other layers, including those between asphalt layers and granular base or substructure layers. This research primarily focuses on examining the effects of geosynthetic reinforcement layers on soft soil increase [3] and [4].

The benefits of employing geosynthetics for the reinforcement of base and sub-base layers have been substantiated by both field and laboratory investigations conducted by scholars [5], [6], [7], and [8]. Research indicates that the shear of soil enhanced with one or more layers of reinforcement is influenced by factors such as the internal failure mode the spacing of the reinforcement elements and the permeability characteristics of the reinforcing materials as evidenced by triaxial compression tests performed on soil integrated with geosynthetic layers.

A comprehensive investigation was performed to assess the mechanical properties, elastic deformations, and permanent deformation characteristics of both pavement and subgrade materials using cyclic triaxial testing that replicate traffic loading scenarios [9]. The research examined a range of variables, including grain size distribution, material density, moisture levels, reinforcement spacing, and the proportion of crushed gravel particles, initial effective stress, and the conditions of cyclic loading, which encompassed static, spherical, and distorting stress components [10]. These variables were critical for establishing design parameters. The outcomes of the laboratory tests were meticulously analyzed and recorded, accompanied by a cost-benefit evaluation. Utilizing the AASHTO pavement design methodology, the necessary combined load-bearing capacity of the pavement layers above the sub-grade was determined. Additionally, a framework for AASHTO geosynthetic reinforced roadway design was established. A comparative analysis of pavement design parameters was conducted for unreinforced and reinforced pavements under various sub-grade conditions. The cost analysis revealed substantial savings associated with reduced substructure strength requirements [11], and [12].

2. Materials & Method

The objective of this study is to forecast both the elastic and permanent deformations of pavement structures in relation to the number of loading cycles and the specific loading conditions applied. The research included a thorough examination of the physical and mechanical properties of the granular base, sub-base materials, and sub-grade soil. CBR and triaxial tests were carried out at the Soil Mechanics Laboratory (LSM) within the Faculty of Civil Engineering at Qom University of Technology. A variety of tests were executed under different loading conditions and repeated loading scenarios [13], [14] and [15]. The granular base material was enhanced by integrating geosynthetic reinforcements and was compacted in a mould to achieve the desired density and moisture content.

3. Flexible Pavement Models

The vertical movement of the pavement is considered a result of the deformations that take place within the pavement layer as well as the underlying sub-grade material. This analysis includes both elastic and permanent deformations related to the road layers and sub-grade, taking into account different stress conditions. The resilient strain is identified as indicative of the elastic strain.

$$M_r = \frac{\Delta\sigma_d}{\Delta\varepsilon_a{}^r} \tag{1}$$

The elastic response of unbound granular materials during cyclic triaxial testing can be characterized using the k-Θ model [4]. The formulation is as follows:

$$E^r = K_1 \cdot \left(\frac{\sigma_1 + 2.\sigma_3}{p_a}\right)^{k_2} = k_1 \cdot \left(\frac{3.p}{p_a}\right)^{k_2} \tag{2}$$

Where

- $\sigma_d, \sigma_1, \sigma_3$ = cyclic deviatoric stress, principal stresses
- $\varepsilon_a{}^r$ = resilient axial strain
- E^r = resilient modulus
- p, p_a = mean normal stress, reference stress (101 kPa)
- k_1, k_2 = model parameters

In this context, Poisson's ratio υ is considered a constant. The k-Θ model can be applied along a designated stress path to effectively tackle elastic problems. Conversely, inelastic issues are addressed using a constant Poisson's ratio υ in conjunction with Young's modulus E. The characterization of volume strains $\varepsilon_v{}^r$ and shear

J. of Science and Technology Vol. 16 No. 2 (2024) p. 71-84

strains $\varepsilon_q{}^r$, along with the moduli E, K, and G, is derived from the research conducted by Dondi [5]. The shear strains ε_q are defined as follows:

$$\varepsilon_q = \frac{p_a{}^{1-n}.p_r{}^n}{3.G_a}.\left(\frac{q_r}{p_r}\right)^2 \tag{3}$$

Where

- p_a = constant stress (100 kPa)
- p_r = mean normal stress
- q_r = deviator stress
- G_a= parameter of model

The modulus of elasticity is influenced by both the mean and deviatoric stresses. Taking these factors into account, Ling [6] explored a novel model. The revised AASHTO equation designed to represent this behavior has been incorporated.

$$M_r = k_1.б_a.\left(\frac{\sigma_1 + 2.\sigma_3}{\sigma_a}\right)^{k_2}.\left(\frac{\tau_{oct}}{\sigma_a} + 1\right)^{k_3} \tag{4}$$

Where

- σ_a = reference stress (101 kPa)
- ε_1,σ_3 = principal stresses
- τ_{oct} = octahedral shear stress
- k_1,k_2,k_3 = model parameters

The assessment of permanent deformations in EFG materials relies on cyclic testing as outlined in standards [7] and [9], which exhibit variations in certain specifics.
The limit state plastic strains are calculated in agreement with the Nazzal model [8]. The relation between the axial permanent deformations $\varepsilon_1{}^p$ (N).

$$\varepsilon_1{}^p(N) = \varepsilon_1{}^{p^*}(N) + \varepsilon_1{}^p(100) \tag{5}$$

Where

- $\varepsilon_1{}^p$ (100) = axial permanent deformation after 100 cycles
- $\varepsilon_1{}^{p^*}$(N) = normalized axial permanent deformation at N > 100

Equation 6 illustrates the normalized axial permanent deformation, with parameters A and B characterizing the increase in strain relative to the number of loading cycles. Parameter A represents the threshold of the permanent axial deformation function, while parameter B indicates the degree of deflection. The variations in axial permanent deformation ε_1 and normalized axial permanent deformation $\varepsilon_1{}^{p*}$ are expressed as a function of the loading cycle count N.

$$\varepsilon_1{}^{p^*} = A.F(N) = A.\left[1 - \left(\frac{N}{100}\right)^{-B}\right] \tag{6}$$

The magnitude of parameters A and B depend on the stress level, which is expressed by the spherical and deviatoric stress components

$$p = \sigma_0 + \frac{\sigma_1 + 2.\sigma_3}{3} \quad q = \sigma_1 - \sigma_3 \tag{7}$$

The change in the plastic strain with the loading cycles is

$$\frac{d\varepsilon^p}{dN} = \frac{\varepsilon_1{}^{p^*}}{dN} = \frac{A.B}{N}.\left(\frac{N}{100}\right)^{-B} \tag{8}$$

The maximum axial permanent deformation or parameter *A* is proportional to the maximum deviatoric and spherical stresses given in Equation 6.

$$A = \frac{\frac{q_{max}}{(p_{max} + p^*)}}{a - b.\frac{q_{max}}{(p_{max} + p^*)}} \tag{9}$$

Where the stress parameter p* is defined by the intersection of the failure line with the q-axis in p-q space. It is determined from the linear equation of the test data using the least squares method.

$$q = k.p - p^* \tag{10}$$

Where *k* is the slope of the failure line. Parameters a and b are determined from the test data, with linear equation of the inverse value of parameter *A,* using the method of the least square deviation.

$$A^{-1} = a.\left[\frac{q_{max}}{p_{max} + p^*}\right]^{-1} - b \tag{11}$$

The relation between parameters *a* and *b* gives the slope of the failure line, given by parameter *M*

$$M = {}^{a}/_{b} \tag{12}$$

The failure line in the *p-q* space is

$$q = M.(p + p^*) \tag{13}$$

The development of the permanent axial deformations in the p-q space can be given by

$$\varepsilon_1{}^{p^*}(N, \rho, w, p, q) = \varepsilon_0.f(\rho).f(w).f(p).f(q) \tag{14}$$

Where the characteristic value of the permanent axial deformation ε_0 is given at selected values of the spherical stress component p_0 and the deviatoric stress component q_0

$$\varepsilon_0 = \varepsilon_1{}^{p^*}(N_0, \rho_0, w_0, p_0, q_0) \tag{15}$$

The magnitude of the permanent axial deformation depends on the spherical stress component *p* and the deviatoric stress component *q*, following the exponential equation

$$\varepsilon_1{}^{p^*}(N, p, q) = \varepsilon_0.e^{C\left(1-\left(\frac{p}{p_0}\right)^D\right)}.e^{\left(1-\left(\frac{q}{q_0}\right)^F\right)} \tag{16}$$

Where C and D are the parameters defining the variations of the normalized permanent axial strain $\varepsilon_1{}^{p^*}$ as a function of the spherical stress component p, E and F are parameters defining the variations of the permanent axial strain as a function of the deviatoric stress component q.

The fluctuations in additional factors, such as density and water content, can also be articulated. Given the negligible alterations in these parameters across different material types, they are regarded as stable conditions. From equation 14, the normalized permanent axial deformation $\varepsilon_1{}^{p^*}$ is expressed in terms of the spherical stress component p and the deviatoric stress component q, which can be specified with the surface in $\varepsilon_1{}^{p^*}$ - p - q space.

At a certain constant value of the spherical stress component p, the value of $\varepsilon_1{}^{p^*}$ increases exponentially with increasing q, and at a certain limit the value of q diverges. For any plane in $\varepsilon_1{}^{p^*}$ - p - q space with any value of p, the relationship between the deviatoric stress component q and the normalized permanent axial strain $\varepsilon_1{}^{p^*}$ can be determined [10].

$$q\left(\varepsilon_1{}^{p^*}\right) = q_0.\left[1 + \frac{1}{E}.In\left(\frac{1}{e^{C\left(1-\left(\frac{p}{p_0}\right)^D\right)}}\frac{\varepsilon_1{}^{p^*}}{\varepsilon_0}\right)\right]^{1/F} \tag{17}$$

As the spherical stress component p rises and the deviatoric stress component q remains constant, the value of $\varepsilon_1{}^{p^*}$ approaches a specific limit. Equations 16 and 17 can be employed to ascertain the failure and deformation curves within the p-q space.

J. of Science and Technology Vol. 16 No. 2 (2024) p. 71-84

4. Repeated Load Triaxial Tests

This paper investigates triaxial repeated loading tests performed on unbound mixtures using two different approaches: the variable confining pressure method, where the cell pressure is cyclically adjusted during the vertical axial loading phase, and the constant confining pressure method, in which the cell pressure remains constant while the vertical axial load is varied cyclically. The study includes a series of individual tests conducted along various stress paths, with the applied stresses being gradually increased. The ratio of distortional to spherical stresses, represented as q/p, varies from 0 to 3 for each test. The experiments are conducted with a limited number of cycles (N=100) after a conditioning phase of 20,000 cycles to evaluate the elastic parameters, and with a greater number of cycles (80,000 or more) to examine the characteristics of permanent deformation. The execution of cyclic triaxial tests necessitates the use of specialized testing apparatus, which includes a triaxial cell, a hydraulic press, and various ancillary devices, along with measuring instruments, a control system, a data acquisition system, and the requisite computer hardware and software. The setup of the testing apparatus and the arrangement of reinforcements are depicted in Fig. 1.

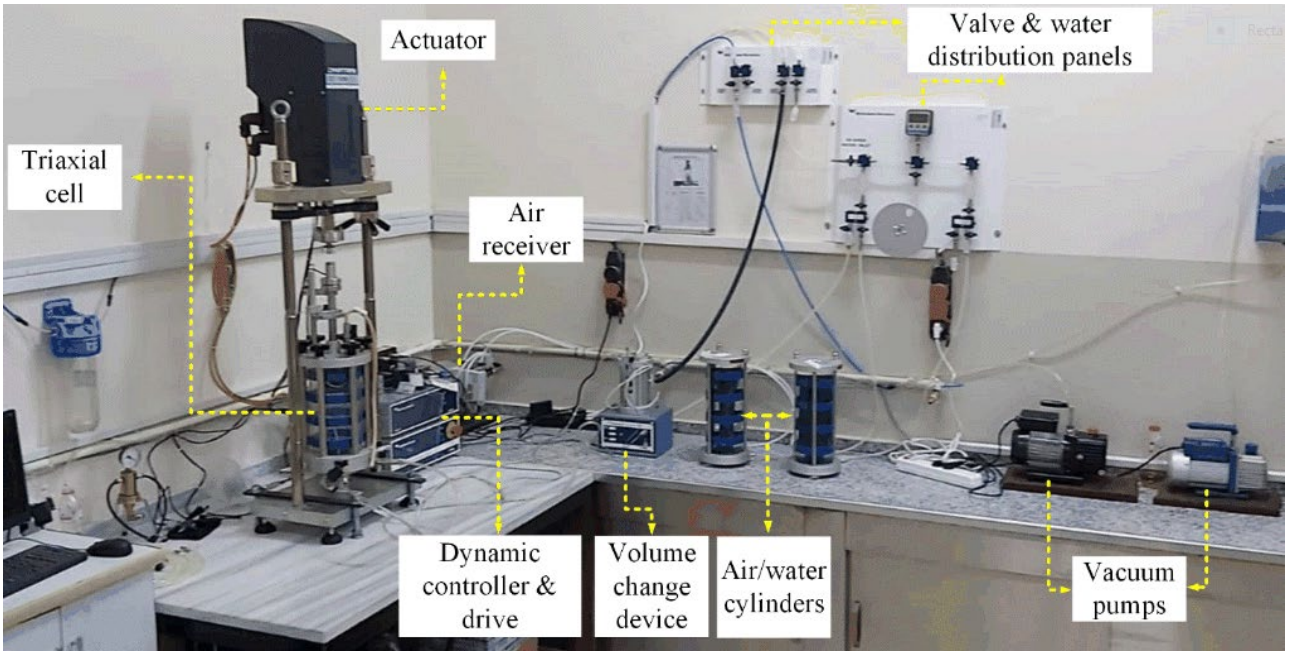

Fig. 1 *Dynamic triaxial test system*

In the present investigation, neither the unreinforced nor the reinforced systems showed any signs of failure. Instead, following 10,000 cycles, the samples exhibited enhanced compactness and density, as depicted in Fig. 2. Some minor necking was observed at the locations of the geosynthetic materials during the testing process, with the most pronounced necking occurring at the upper reinforcement layer. This occurrence can be explained by the bulging of the granular fill located between the geosynthetic layers, even though the geosynthetic effectively restricted the lateral expansion of the specimen.

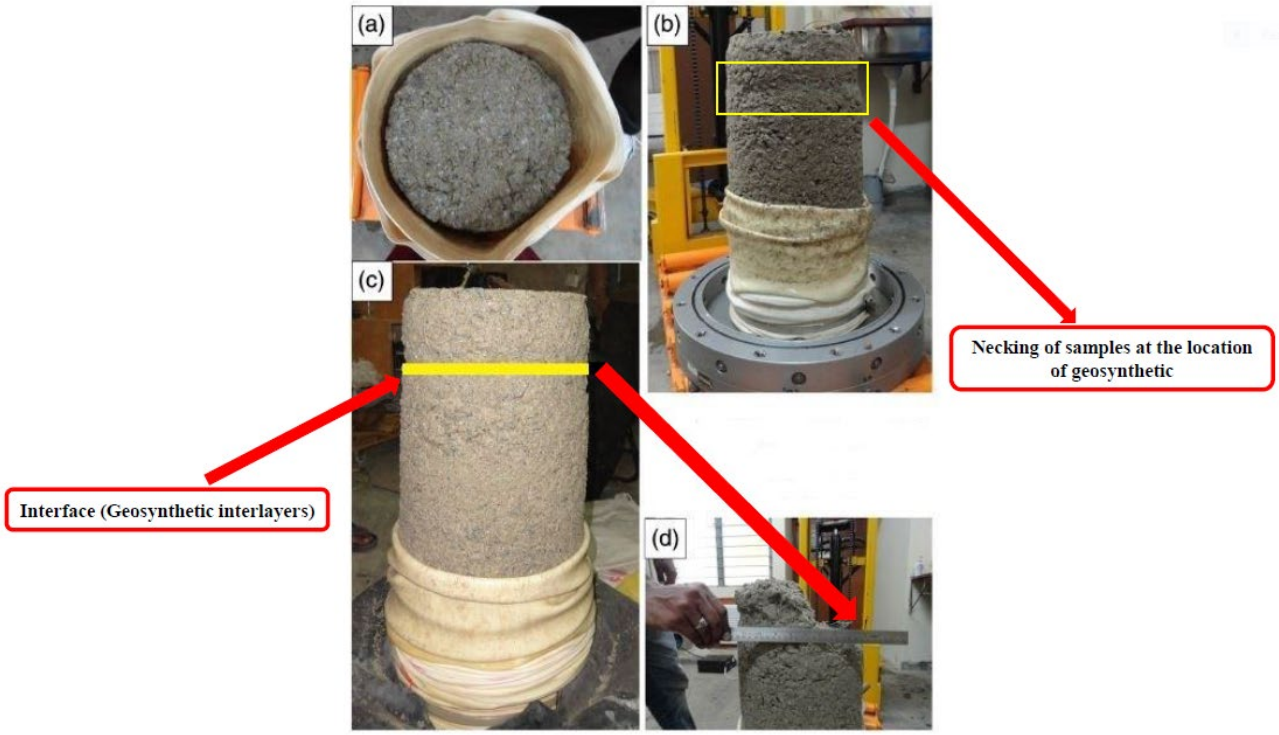

Fig. 2 *Prepared sample reinforced with geosynthetic*

5. Deformation Analysis

After each distinct phase of the investigation, the strength characteristics are calculated based on the recorded deformation and stress parameters. The parameters measured during the tests include cell pressure (σ_3), vertical stress (σ_1), vertical strain (ε_1), and radial strain (ε_3).

The validity of the proposed model was assessed through a practical examination involving repeated load triaxial tests on granular materials used in sub-grade and base courses. Both reinforced and unreinforced samples were subjected to testing. The study also considered the types of stone materials in relation to the proportion of crushed grains present in the gravel and its water content. Investigations into the stone materials for sub-grade and base courses were performed in both laboratory settings and field conditions. The laboratory assessments encompassed:

a) Characteristics of the stone materials (including mineralogical and petrographic composition, presence of hazardous admixtures, mechanical properties, quality assessments, physical properties, and geometric and mechanical attributes of the stone grain mixture),
b) Techniques for enhancing the integration of the stone grain mixture (such as crushing, incorporation of additives like electro filter ash, and soil reinforcement),
c) Repeated load triaxial testing.

A portion of the analysis provided utilizes data derived from the report [16]. The foundational course material underwent testing under repeated loading conditions with a water content set at $w = w_{opt} - 2\%$. The physical characteristics remained consistent across all types of stone materials.

6. Sub-grade Material

A comprehensive assessment of the quality of natural sandy gravel was conducted both in laboratory settings and in situ. Multiple triaxial stress tests were performed, and various samples of stone material were analyzed. The physical characteristics of the analyzed stone material types exhibited variability in accordance with the selected sub-grade strength, as determined by the California Bearing Ratio (CBR). Fig. 3 illustrates some of the apparatus utilized in the CBR testing process. [17]

J. of Science and Technology Vol. 16 No. 2 (2024) p. 71-84

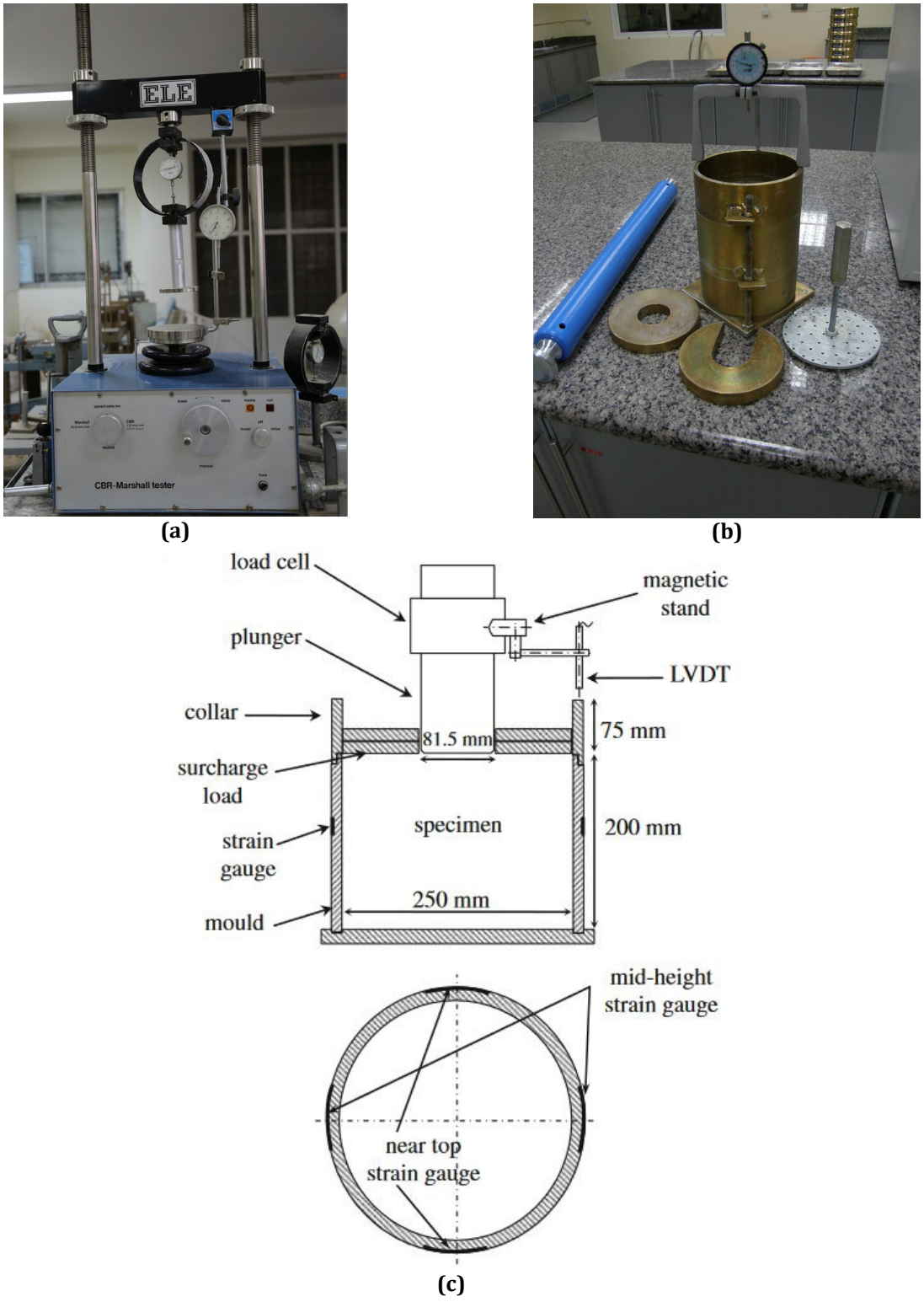

Fig. 3 *(a) CBR test apparatus; (b) The CBR mould and implements in the CBR Test; (c) Schematic diagram*

Samples both with and without reinforcements were subjected to testing. The influence of reinforcements on resilient stiffness and permanent deformations was investigated.

7. Deformation Analysis

The analysis of deformation was conducted through a series of repeated triaxial stress tests on various material types. Fig. 4 illustrates the typical results observed, specifically the increasing strain in the repeatedly loaded

sand-gravel subsoil. In Fig. 5, the results for the sand-gravel subsoil are presented, highlighting the relationship between the deviatoric stress ratio Δ_q and the vertical axial strain ε_1. The parameters A and B were derived from equations (6) and (8), which provide a numerical framework for understanding the progression of permanent axial strains ε_1^p (N) and normalized permanent axial deformations ε_1^{p*} (N) [18] and [19].

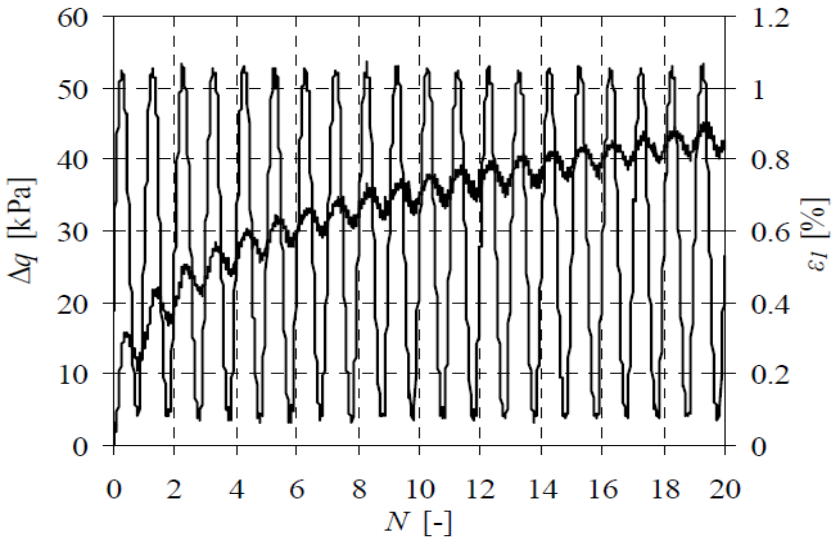

Fig. 4 *Deviatoric stress Δq and vertical axial strain ε_1 vs. time t (number of loading cycles)*

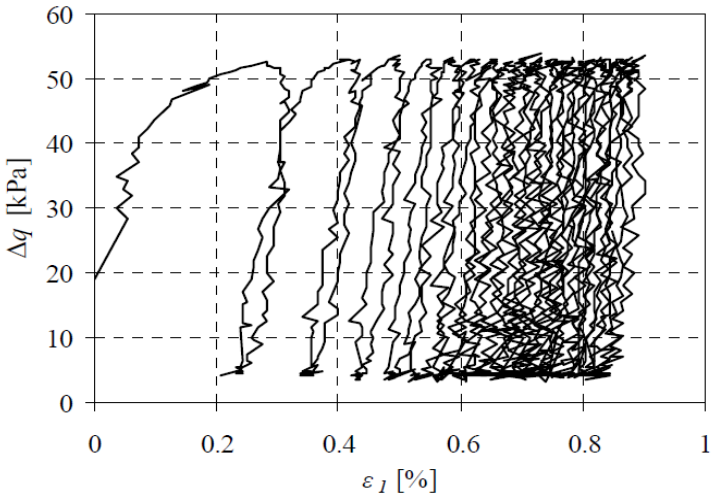

Fig. 5 *Deviatoric stress Δq vs. vertical axial strain ε_1*

Fig. 6 illustrates the relationship between the normalized axial permanent deformation ε_1^{p*} and the number of loading cycles N for the uncrushed variant of base course stone material, characterized by a water content of $w = w_{opt}$ - 2%.

J. of Science and Technology Vol. 16 No. 2 (2024) p. 71-84

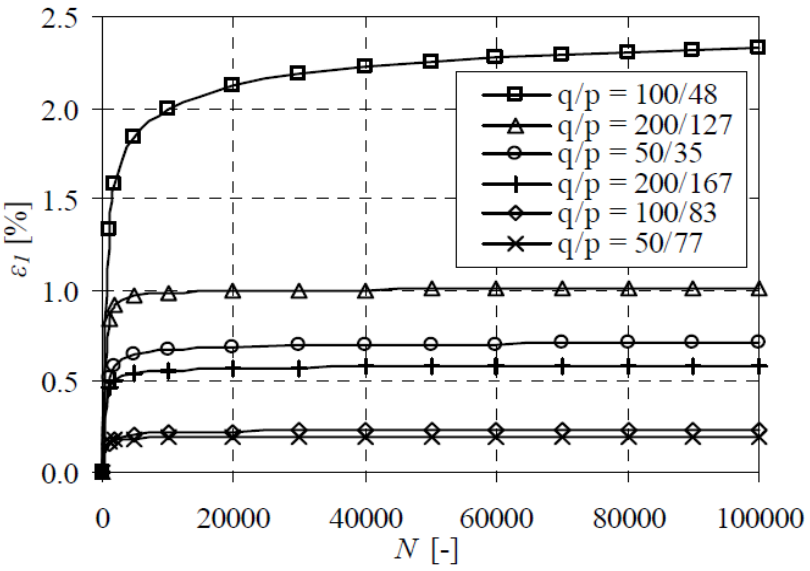

Fig. 6 *Normalised axial permanent deformation ε_1^{p*} vs. the number of loading cycles N for various loadings of stone materials with a water content of w = w_{opt} - 2%*

The behavior of the normalized axial permanent set ε_1^{p*} can be represented as a function of the deviatoric stress q and the spherical stress p across various cycles. This allows for the derivation of the correlation between the normalized axial permanent deformation ε_1^{p*} and the deviatoric stress q, while maintaining a constant spherical stress p, which is analyzed within specific planes of the ε_1^{p*} - p - q space. Fig. 7 illustrates the relationship of the normalized axial permanent strain ε_1^{p*} (N) in relation to the spherical stress p and deviatoric stress q for the subsurface material [20].

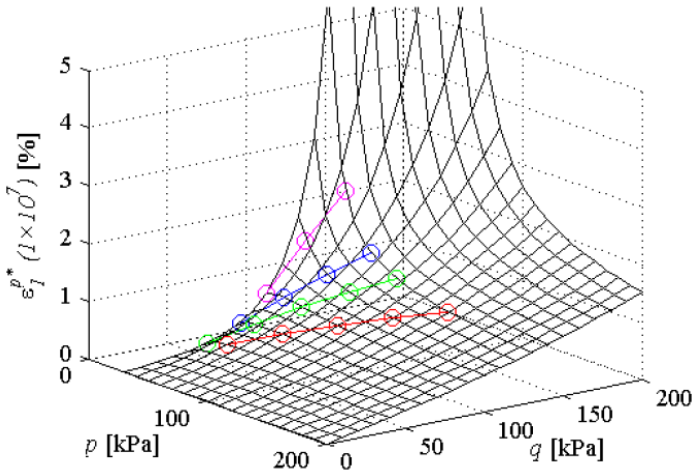

Fig. 7 *Sub-grade normalized axial permanent deformation ε_1^{p*} in the ε_1^{p*} - p – q space.*

The correlation between the normalized axial permanent deformation ε_1^{p*} and the distortional stress q, under a constant spherical stress p, was derived from equations 15 and 16, as illustrated in the ε_1^{p*} - p – q space. Fig. 8 presents these relationships specifically for the base course material. By applying equations 10 to 13, it is possible to determine the failure envelopes within the p – q space for various types of stone materials [21].

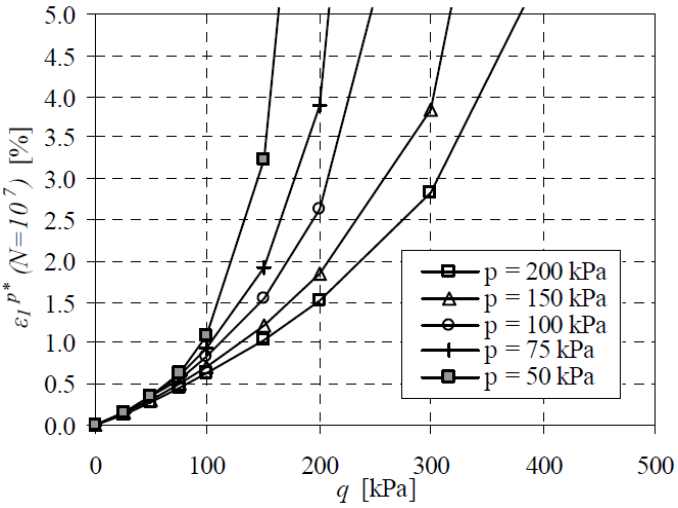

Fig. 8 *Normalized axial permanent deformation $\varepsilon_1^{p^*}$ vs. distortional stress q for various constant spherical stresses p*

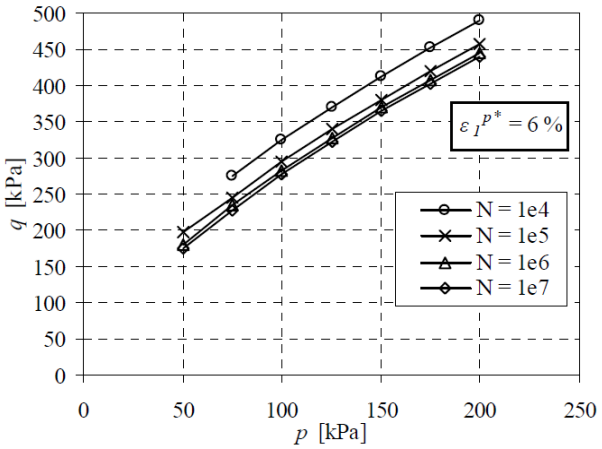

Fig. 9 *Deformation envelopes for various numbers of loading cycles N*

The connection between the spherical stress component p and the deviatoric stress component q at a given level of normalized axial permanent strain ε1p* leads to the formation of deformation envelopes. These strain envelopes diminish as the number of cycles N rises, but they expand with increased axial fatigue strain, ultimately nearing the failure envelope that characterizes the critical state of the q/p relationship (Fig. 9).

Fig. 10 shows failure envelopes for unreinforced and reinforced sub-grade material compared to base course material.

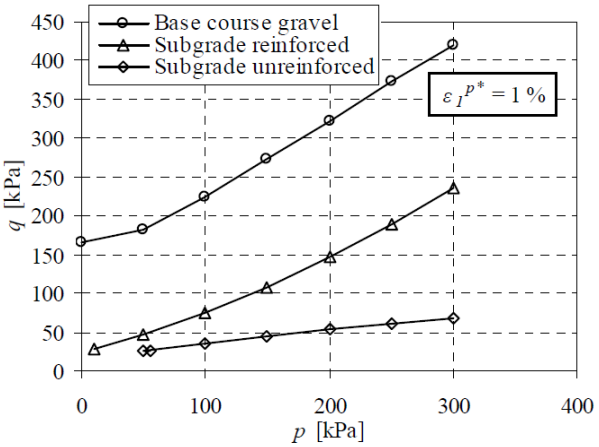

Fig. 10 *Failure envelopes for unreinforced and reinforced sub-grade and base course material*

J. of Science and Technology Vol. 16 No. 2 (2024) p. 71-84

8. Analysis of Pavement Structure

A finite element method (FEM) was employed to conduct an elastic-plastic analysis, aimed at comparing the findings with experimental results and establishing the parameters necessary for the FEM analysis of the pavement. Fig. 11 illustrates the two-dimensional finite element mesh utilized in the examination of geosynthetic-reinforced pavement models. The outcomes of the elastic-plastic analysis, which include axial force, horizontal deformation, and shear stress, indicate significant variations in results when reinforcement is applied. The elastic-plastic analysis of a flexible pavement structure consists of three distinct phases:

a) Specification of the mesh, material properties, loading conditions, and boundary constraints for the finite elements.
b) Calculation of plastic displacements and strain components.

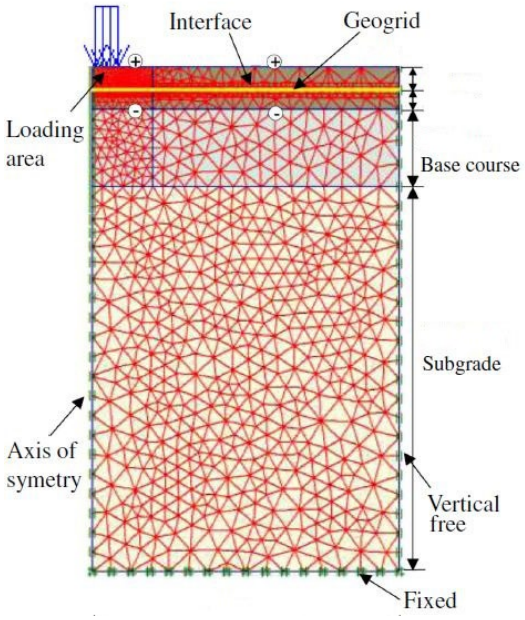

(a)

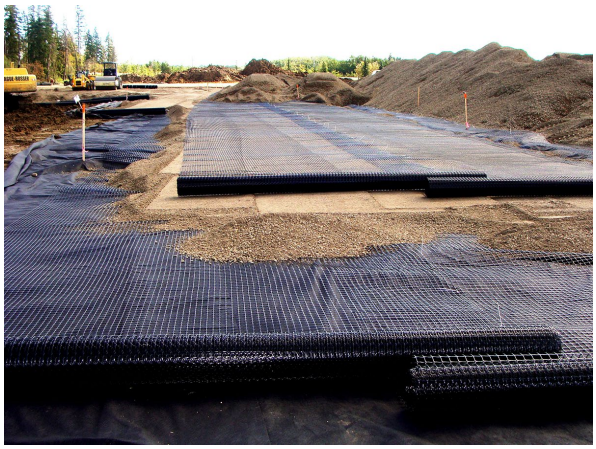

(b)

(c)

Fig. 11 *(a) Finite Element Meshed Geosynthetic-Reinforced Pavement Model; (b) and (c) Geosynthetics used in the study*

The connection between the subsoil height CBR and the load count N is determined to achieve specific rut depths of 10 mm and 20 mm across different gravel layer thicknesses, which can be either reinforced or

unreinforced. Utilizing the principles from the AASHTO flexible pavement design methodology, the required combined load-bearing capacity of the pavement layers above the sub-grade is calculated. Fig. 12 displays the necessary thickness of the base course for various substrate thicknesses and different traffic conditions, including light, medium, and heavy traffic scenarios [22].

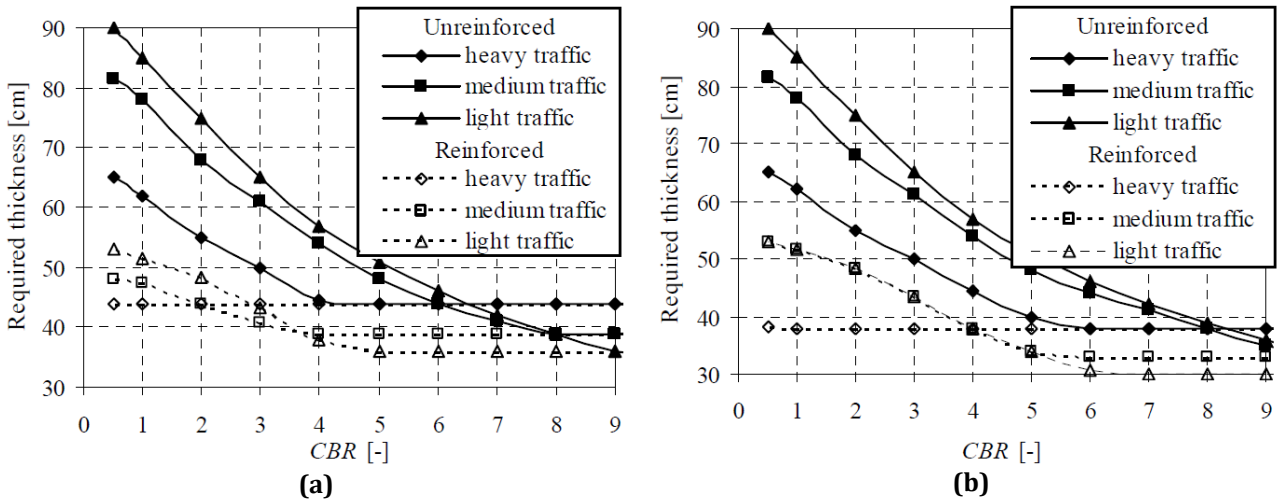

Fig. 12 *Thickness of base layer d vs. sub-grade strength CBR for (a) 80; and (b) 90 cm freezing zones*

9. Cost-saving Analysis

An average expense of 15 EUR for an engraved aggregate base and 1.2 EUR for engraved geosynthetic reinforcement has been employed to calculate the savings associated with the use of reinforcements across varying sub-grade strengths. Fig. 13 illustrates the cost savings per square meter for pavements incorporating reinforcements, considering different sub-grade strengths and traffic loads within 80 and 90 cm freezing zones.

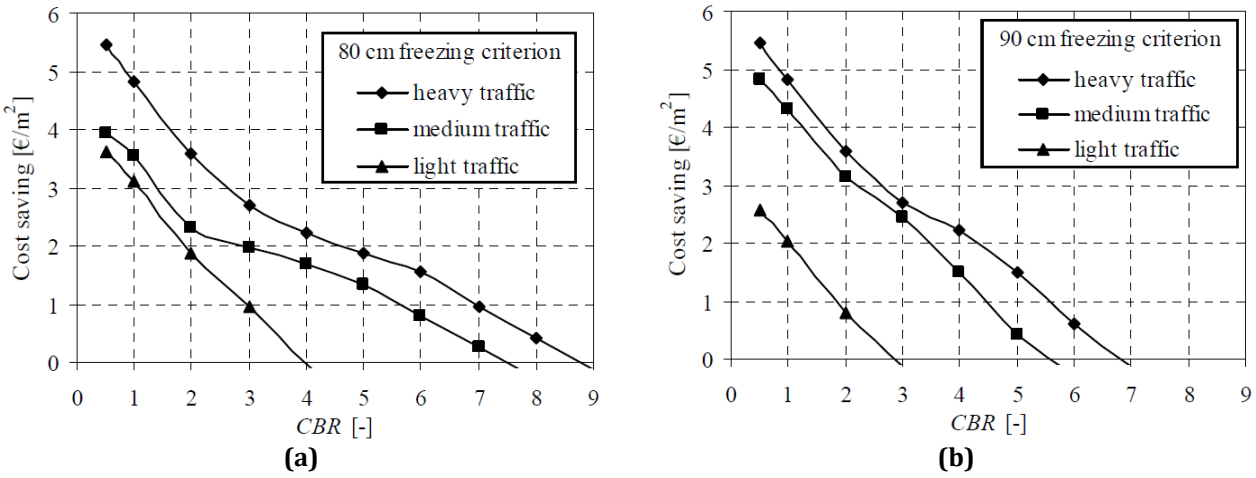

Fig. 13 *Cost savings vs. sub-grade strength CBR for (a) 80; and (b) 90 cm freezing zones*

10. Conclusions

A thorough series of experiments was carried out to assess different stress states and dynamic loading conditions. The base and sub-base materials were improved with geosynthetic reinforcements and compacted in a mold to achieve specific density and moisture levels. Two types of samples were examined: one group without reinforcement and another with reinforcement. The study included a variety of tests in which parameters such as density, moisture content, effective initial stress, and cyclic loading were systematically altered.

A variation in material stiffness was observed during cyclic loading. The modulus of elasticity was defined using the AASHTO 2002 PDG model. It was found that the reinforcement does not have a significant impact on elastic stiffness. The reinforced samples exhibited a notable decrease in permanent sets when compared to the unreinforced samples. Permanent deformations are characterized by the number of load cycles (N), the

spherical component of cyclic loading (p), and the deformation component of cyclic loading (q). These findings can be illustrated through deformation and failure envelopes for any specified number of cycles (N). To facilitate a comparison of the test outcomes and establish the parameters necessary for a finite element method (FEM) analysis of pavement, an elastic-plastic analysis was conducted utilizing FEM. By integrating the principles of the AASHTO flexible pavement design methodology, the requisite combined load-bearing capacity of the pavement layers situated above the sub-grade was determined. Additionally, a design approach for geosynthetically reinforced pavements based on AASHTO guidelines was formulated. The design parameters for both unreinforced and reinforced pavements, as well as various subsoil conditions, were analyzed. Furthermore, a cost-benefit analysis was performed, revealing substantial savings associated with lower sub-grade strength.

Acknowledgement

The authors would like to thank the Department of Civil Engineering, Qom University of Technology, Tehran, 1651958171, Iran for allowing to conduct this research.

Conflict of Interest

Authors declare that there is no conflict of interest regarding the publication of the paper.

Author Contribution

The author confirms sole responsibility for the following: study conception and design, data collection, analysis and interpretation of results, and manuscript preparation.

References

[1] Austin, R. A., and A. J. T. Gilchrist. (1996) Enhanced performance of asphalt pavements using geocomposites. *Geotextiles and Geomembranes*. 14 (3–4): 175–186. https://doi.org/10.1016/0266-1144(96)00007-610.

[2] Abu-Farsakh, M., and Q. Chen. (2011) Evaluation of geogrid base reinforcement in flexible pavement using cyclic plate load testing. *International Journal of Pavement Engineering*. 12 (3): 275–288. https://doi.org/10.1080/10298436.2010.549565.

[3] Abu-Farsakh, M. Y., J. Gu, G. Z. Voyiadjis, and Q. Chen. (2014) Mechanistic–empirical analysis of the results of finite element analysis on flexible pavement with geogrid base reinforcement. *International Journal of Pavement Engineering*. 15 (9): 786–798. https://doi.org/10.1080/102984362014.893315.

[4] Brinkgreve, R. B. J., and P. A. Vermeer. (1998) PLAXIS finite element code for soil and rock analyses. Rotterdam, Netherlands: A. A. Balkema. https://www.scirp.org/reference/referencespapers?referenceid=2672279

[5] Dondi, G. (1994) Three-dimensional finite element analysis of a reinforced paved road. In Proc., 5th International Conference on Geotextiles, Geomembrane and Related Products, 95–100. Singapore: International Geotextile Society. https://www.tib.eu/en/search/id/BLCP%3ACN007877780/Three-Dimensional-Finite-Element-Analysis-of-a/

[6] Ling, H. I., and Z. Liu. (2001) Performance of geosynthetic-reinforced asphalt pavements. *Journal of Geotechnical and Geoenvironmental Engineering*. 127 (2): 177–184. https://doi.org/10.1061/(ASCE)1090-0241(2001)127:2(177).

[7] Pandey, S., R. K. Rao, and D. Tiwari. (2012) Effect of geogrid reinforcement on critical responses of bituminous pavements. In Proc., 25th ARRB Conf. Shaping the Future: Linking Policy, Research and Outcomes, 17. Exton, PA: ARRB Group Ltd. https://trid.trb.org/view/1224083

[8] Nazzal, M., M. Abu-Farsakh, and L. Mohammad. (2010) Implementation of a critical state two-surface model to evaluate the response of geosynthetic reinforced pavements. *International Journal of Geomechanics*. 10 (5): 202–212. https://doi.org/10.1061/(ASCE)GM.1943-5622.0000058

[9] Ramazan Borujerdi, A., and Jiryaei Sharahi, M. (2018) Seismic Bearing Capacity of Strip Footings Adjacent to Slopes Using Pseudo Dynamic Approach (Summary of MSc Thesis). Master of Science Thesis, Qom University of Technology. http://dx.doi.org/10.13140/RG.2.2.30142.15686.

[10] Ramazan Borujerdi, A., and Jiryaei Sharahi, M. (2021) Seismic Bearing Capacity of Strip Footings Adjacent to Slopes Using Pseudo Dynamic Approach. *Journal of Mathematics and Computational Sciences*, 2(1), pp. 17–41. https://dx.doi.org/10.30511/mcs.2021.137964.1009.

[11] ASTM. (2015) Standard test method for determining tensile properties of geogrids by the single or multi-rib tensile method. ASTM D6637. West Conshohocken, PA: ASTM. https://cdn.standards.iteh.ai/samples/92011/1f3fb41af79c4f0182cafeb37d83140b/ASTM-D6637-D6637M-15.pdf
[12] Perkins, S. W. (2001) Mechanistic–empirical modeling and design model development of geosynthetic reinforced flexible pavements. Rep. No. FHWA/MT-01- 002/99160-1A. Helena, Montana: Montana Dept. of transportation. https://rosap.ntl.bts.gov/view/dot/44037
[13] Ramazan Borujerdi, A. (2023) Site Characterization of Alluvial Silty Sand Soils by Dynamic In-Situ and Laboratory Tests. *International Journal of Sustainable Construction Engineering and Technology*, 14(1), 260–269. https://doi.org/10.30880/ijscet.2023.14.01.023
[14] Ramazan Borujerdi, A. (2023) Numerical and Experimental Analysis of Seismic Soil Pile Structure *Interaction. Emerging Advances in Integrated Technology*, 3(2), 1–10. https://doi.org/10.30880/emait.2022.03.02.001
[15] ASTM. (2015) Standard Practice for Classification of Soils and Soil aggregate Mixtures for Highway Construction Purposes. ASTM D3282. West Conshohocken, PA: ASTM. https://cdn.standards.iteh.ai/samples/92993/33eb868df69f4cd28f6d4f821cfed90e/ASTM-D3282-15.pdf
[16] Paterson, W. D. O. (1987) Road deterioration and maintenance effects: Models for planning and management. Washington, DC: World Bank. https://documents1.worldbank.org/curated/en/222951468765265396/pdf/multi-page.pdf
[17] Solaimanian, M. (2013) Evaluating resistance of hot mix asphalt to reflective cracking using geocomposites. Rep. No. PSU-2008-04. State College, PA: Pennsylvania State Univ. https://rosap.ntl.bts.gov/view/dot/25807
[18] Ling, H., and H. Liu. (2003) Finite element studies of asphalt concrete pavement reinforced with geogrid. *Journal of Engineering Mechanics*.129 (7): 801–811. https://doi.org/10.1061/(ASCE)0733-9399(2003)129:7(801).
[19] RamazanBorujerdi, A. (2023) Analysis of Geosynthetic – Reinforced Stone Piles – Supported Embankments. *Journal of Sustainable Underground Exploration*, 3(1), 35-41. https://doi.org/10.30880/jsue.2023.03.01.006
[20] Jegatheesan, P., & Gnanendran, C. T. (2015) Permanent deformation study of pavement layers using laboratory pavement odel testing. *International Journal of Geomechanics*. 16(3), 04015072. https://doi.org/10.1061/(ASCE)GM.1943-5622.0000606
[21] Rahman, M. S., & Erlingsson, S. (2015) Predicting permanent deformation behaviour of unbound granular materials. *International Journal of Pavement Engineering*, 16(7), 587–601. https://doi.org/10.1080/10298436.2014.943209
[22] Yang, S. R., & Chang, J. R. (2016) Using genetic programming to predict plastic strain in sub-grade soils under repeated loading. *Journal of Testing and Evaluation*. 45(1), 85–93. https://doi.org/10.1520/JTE20160128